Comparison between blade-element models of propellers

O. Gur and A. Rosen
Technion Israel Institute of Technology
Haifa, Israel

ABSTRACT

Blade-element models are the most common models for the analysis of propeller aerodynamics, performance calculations and propeller design. In spite of their simplicity these models are very efficient and accurate. Blade-element models use the local induced velocities as an input thus they should be combined with another model in order to calculate these induced velocities. Various models are used for the calculation of the induced velocity, where the most popular ones include: momentum, simplified-momentum, lifting-line (prescribed and free wake), and vortex (McCormick and Theodorsen) models. The paper describes the various models, compares their results and discusses the advantages and disadvantages of each one. The results indicate that the Blade-element/simplified-momentum model offers very good accuracy together with high efficiency. For propeller performance calculations during steady axial flight, where most of the cross-sections do not experience stall, detailed and complicated models for calculating the induced velocities do not show advantages over the simple blade-element/simplified-momentum model,

NOMENCLATURE

c	chord
C_l, C_d	2D lift and drag coefficients
$\widetilde{C}_l$	corrected two dimensional lift
C_T, C_P	thrust and power coefficients, respectively
D	propeller diameter
D'	drag per unit length of the blade
J	advance ratio
K	Theodorsen's circulation function
l_B	co-ordinate along the blade cross-sectional quarter chord points
L'	lift per unit length
M	Mach number
n	propeller's angular speed (revolutions per second)
N_b	number of blades
p'	pressure at the far wake
Δp	pressure jump across the actuator disk
p_1, p_2	pressure of the flow entering and exiting the actuator disk, respectively
p_a	ambient pressure
P_z	wake helical pitch
dQ	torque of disk annulus
r	radial co-ordinate at the disk plane
r'	radial co-ordinate at the far wake
Re	Reynolds number
dT	thrust of disk annulus
x_B, y_B, z_B,	blade's cross-sectional co-ordinates
V_{a-BE}, V_{t-BE}	axial and circumferential incoming cross-sectional velocities, respectively
V_{BE}	resultant cross-sectional velocity
V_F	vehicle's flight velocity
w	displacement velocity
w_a, w_t, w_r	axial, circumferential, and radial induced velocity components, at the disk plane
w'_a, w'_t	axial and circumferential induced velocity components in the far wake
w_{a-BE}, w_{t-BE}	axial and circumferential induced velocity components at the cross-section
w_{a-Wake}	axial induced velocity in the wake

Paper No. 3277. Manuscript received 17 January 2008, revised 5 August 2008, second revision 26 August 2008, accepted 11 September 2008.

https://doi.org/10.1017/S0001924000002669 Published online by Cambridge University Press

Y	Theodorsen's contraction factor
α	angle-of-attack
β	pitch angle
$\beta_{0.75}$	pitch angle at 75% of blade radius
Γ_B, Γ_T	circulation of the bound and trailing vortex filaments, respectively
Γ_∞	bound circulation for infinite number of blades
ϕ	inflow angle
κ	Goldstein's coefficient of interference velocity
λ	advance ratio of the far wake
ρ_a	air density
σ	solidity
Ω	propeller's angular speed

1.0 INTRODUCTION

The aerodynamic analysis of rotary wings (propellers, rotors, and wind turbines) has been developed during the last hundred years. CFD codes present the most comprehensive methods of analyzing rotary wings. These codes have many advantages, like their ability to analyze planform effects or capture compressibility and viscosity effects. CFD analyses are used to investigate complex phenomena such as blades that experience stall along large portions[1] or propeller-fuselage interaction[2]. Initially the use of CFD methods to investigate propeller aerodynamics was limited because of the large computer resources that were required[3-4]. Due to developments of hardware and codes, nowadays a propeller in axial flight can be resolved, using full RANS simulation, within hours of CPU time on a modern personal computer, Yet, this is too expensive and time consuming for many applications such as design optimisation or real time simulation.

Veteran blade-element models are commonly used for the aerodynamic analysis of rotary wings, including propellers. The Wright brothers were probably the first to use a crude blade-element model in order to design a propeller for their Wright-flyer. The proper design of their propeller was probably one of the main reasons for their success in accomplishing the first flight of a heavier than air vehicle[5]. Drzewiecki[6] was probably the first to introduce a modern blade-element model. Since then blade-element models are commonly used for the analysis and design of propellers[7].

The main advantages of the various blade-element models are their simplicity, accuracy and low demand of computer resources. Blade-element models are especially suitable for design processes or simulations involving a large number of calculations that require high accuracy as well as numerical efficiency.

Blade-element models are based on dividing each propeller's blade into small elements (segments). It is assumed that each element behaves aerodynamically as a wing in a two-dimensional flow. The element lift and drag coefficients are functions of: the local angle-of-attack, Mach number, and Reynolds number. These parameters are functions of the cross-sectional resultant velocity, which is obtained by summing up all the following contributions: the air-vehicle flight velocity, rotation of the blade, and induced velocity. While the flight velocity and rotational velocity are known, the induced velocity components are unknown. To find these unknowns, another model should be used together with the blade-element-model. Over the years various models have been used for that purpose, including: momentum models[8], lifting-line models[9], and vortex models[10,11]. These models allow the calculation of the induced velocity by using different approaches.

The momentum model, uses an actuator disk[12] approach where the flow field is divided into concentric annuli control volumes. The lifting-line is a somewhat more complex model which is based on Prandtl's lifting-line theory[13] and includes different approaches to calculating the wake geometry[9,14]. Vortex models (represented here by Theodorsen's and McCormick's models) are based on the optimal distribution of the blade's circulation and the Kutta-Joukowski theorem.

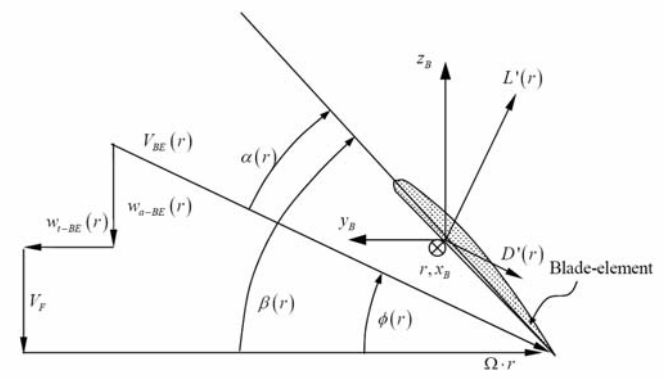


Figure 1. Cross-section of a blade-element of a propeller having straight blades, at axial flight.

The cross-sectional components of the induced velocity which are calculated by one of the above mentioned methods become an input to the blade-element model. By using the blade-element model, the aerodynamic loads along the blade are calculated. Usually an iterative process is required in order to obtain convergence. Integration of the aerodynamic loads along the blades results in the propeller's thrust and required power.

Many researchers have used the various above mentioned models and reported their results. Yet, the authors are not aware of any publication where the various models have been compared. The purpose of the paper is to present such a comparison that can help any user to decide which model to use based on his/her needs.

2.0 THE BLADE-ELEMENT MODEL

Usually blade-element models are developed for a propeller in axial flight (the axis of rotation is parallel to the free stream direction), that has straight blades. The blades are divided into small elements in the radial direction. It is assumed that each element behaves as a two dimensional wing. Another assumption is the absence of interaction between neighbour elements. The validity of this assumption has been shown by Lock and Bateman[15] and others.

Figure 1 shows a cross-section of a blade-element. x_B is the spanwise co-ordinate, which in the case of straight blades is identical to the radial co-ordinate, r. y_B is a co-ordinate perpendicular to the radial co-ordinate and parallel to the plane of rotation.

The cross-sectional velocity components are shown in Fig. 1:

(a) The free stream velocity, V_F

(b) Rotational velocity, $\Omega \cdot r$. Ω is the angular speed of the propeller.

(c) Cross-sectional induced velocity. The induced velocity is described by its two cross-sectional components: the axial component, w_{a-BE}, and the circumferential one, w_{t-BE}.

While the first two components are functions of the flight conditions (flight velocity and the propeller's angular speed), the induced velocity components are unknown. In order to find these unknowns, another model should be coupled with the blade-element model, as it will be described in the following sections.

If all the components of the cross-sectional velocity are known, the resultant cross-sectional velocity, V_{BE}, can be calculated. The direction of this cross-sectional velocity defines the inflow angle, ϕ. The angle-of-attack, α, is obtained by subtracting the inflow angle, ϕ, from the local pitch angle, β. The cross-sectional resultant velocity also defines the cross-sectional Mach number (M) and Reynolds number (Re).

https://doi.org/10.1017/S0001924000002669 Published online by Cambridge University Press

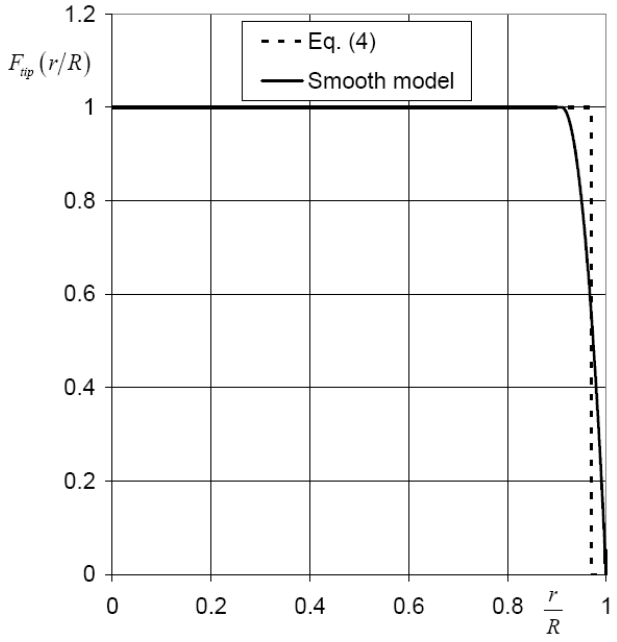


Figure 2. Blade-element tip correction factor.

The cross-sectional lift and drag coefficients, $C_l(\alpha, M, Re)$ and $C_d(\alpha, M, Re)$, respectively, are obtained by using a two dimensional aerodynamic data base. The lift and drag forces per unit length, L' and D', respectively, are:

$$L'(r) = \frac{1}{2}\cdot\rho\cdot V_{BE}(r)^2\cdot c(r)\cdot\tilde{C}_l(r/R,\alpha,M,Re) \quad \ldots (1)$$

$$D'(r) = \frac{1}{2}\cdot\rho\cdot V_{BE}(r)^2\cdot c(r)\cdot C_d(\alpha,M,Re) \quad \ldots (2)$$

ρ is the air density, while c is the chord of the blade-element.

$\tilde{C}_l(r, \alpha, M, Re)$ is the corrected two dimensional lift coefficient of the blade-element, which include the influence of the blade tip:

$$\tilde{C}_l(r/R,\alpha,M,Re) = C_l(\alpha,M,Re)\cdot F_{tip}(r/R) \quad \ldots (3)$$

It is clear that at the propeller tip (last few percents of length) the aerodynamic behaviour is a three dimensional one, where the lift drops to zero at the tip itself[16] $F_{tip}(r/R)$ is a correction factor that accounts for these tip effects.

The simplest correction is to reduce the effective length of the blade[17]:

$$F_{tip}(r/R) = \begin{cases} 0 & \frac{r}{R} > 0.97 \\ 1 & \frac{r}{R} \le 0.97 \end{cases} \quad \ldots (4)$$

In the present case a 'smooth' correction is introduced as shown in Fig. 2. Both corrections give:

$$\int_0^1 F_{tip}(r/R)\cdot d(r/R) = 0.97 \quad \ldots (5)$$

The main difficulty while using blade-element models is the need for a reliable two dimensional aerodynamic data base. This data base should cover all of the combinations of flow conditions experienced by the blades' cross-sections (different combinations of: angles-of-attack, Mach, and Reynolds numbers). Even if such a data base exists, there are additional effects that should be considered, such as the influence of rotation on the nature of cross-sectional stall[18], unsteady and installation effects.

For most operating conditions of propellers, especially those where the cross-sections do not experience stall, blade-element models give good results. Furthermore, using a two-dimensional data base also has its advantages. The two dimensional aerodynamic data base can take into account (at least partially) viscosity effects (through Reynolds number influences) and compressibility effects (through Mach number influences).

The lift and drag per unit length of the element, that are calculated by Equations (1)-(2), are used to calculate the contribution of these elements to the propeller's thrust, dT, and torque, dQ:

$$dT(r) = N_b\cdot\left[L'(r)\cdot\cos\phi - D'(r)\cdot\sin\phi\right]\cdot dr \quad \ldots (6)$$

$$dQ(r) = N_b\cdot\left[L'(r)\cdot\sin\phi + D'(r)\cdot\cos\phi\right]\cdot r\cdot dr \quad \ldots (7)$$

N_b is the number of blades.

As mentioned above, Fig. 1 and the above equations describe the case of axial flight of a propeller that has straight blades. The equations can easily be extended to include the case of swept blades[19], while the following points need special attention:

(a) The velocity components should be projected in a proper manner onto the cross-sectional plane that, in general, is not normal to the local radius. For example, in the case of straight blades the cross-sectional circumferential velocity equals $\Omega\cdot r - w_{t-BE}$, while in the case of swept blades, it also includes a contribution of the radial component of the induced velocity. When the cross-sectional resultant velocity is known, L' and D' are calculated by using Equations (1)-(2).

(b) The contributions of each blade-element to the thrust and torque (dT and dQ, respectively) are calculated using an appropriate transformation of the cross-sectional lift and drag forces to the direction of the propeller axis. Equations (6)-(7) should be corrected accordingly.

The blade-blement model is relatively simple and can easily be implemented, depending on the availability of an appropriate two dimensional aerodynamic data base. As indicated above, the main differences between the various blade-element implementations are the methods of calculating the induced velocity. The most common methods are described in the following sections.

3.0 MOMENTUM MODEL

According to the momentum model, the propeller is replaced by an actuator disk[12] of radius R. The disk has zero thickness and momentum (axial and circumferential) is inserted into the flow that crosses it. According to the momentum model the disk is divided into concentric annuli. The stream lines that pass through the boundary of each annulus, define a set of concentric annular control volumes. Figure 3 shows the pressures and velocity components along a representative control volume. Due to the momentum inserted into the flow, a pressure jump, Δp, is created across the disk. Δp is the difference between the pressure right after the flow exits the disk, p_2, and the pressure just before the flow enters it, p_1. Integration of Δp over the disk results in the total thrust. p_a is the ambient pressure, while p' is the far wake pressure.

The induced velocity through the disk is described by its three components: axial, radial, and circumferential — w_a, w_r, w_t, respectively. The induced velocity in the far wake includes two compo-

https://doi.org/10.1017/S0001924000002669 Published online by Cambridge University Press

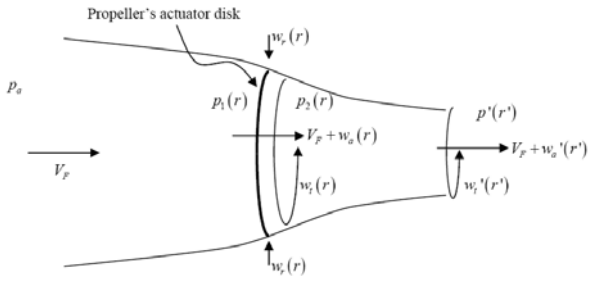


Figure 3. Pressure and velocity components along an annular control volume of an actuator disk.

nents: axial and circumferential, w'_a and w'_t, respectively. The radius of the control volume in the far wake is r' and is a function of the radius of the same control volume while it crosses the disk:

$$r' = r'(r) \qquad \ldots (8)$$

According to the momentum model the interaction between neighbouring control volumes is assumed to be negligible. Based on this assumption and neglecting viscosity effects, the general-momentum equations are obtained[8]:

(a) Conservation of angular momentum in the wake:

$$w_t'\left[r'(r)\right]\cdot r'(r) = w_t(r)\cdot r \qquad \ldots (9)$$

(b) Thrust equation — the relation between the pressure jump across the disk and the contribution of the annulus to the total thrust:

$$\mathrm{d}T(r) = 2\cdot\pi\cdot r\cdot\Delta p(r)\cdot\mathrm{d}r \qquad \ldots (10)$$

(c) Equilibrium of forces in the radial direction, in the far wake:

$$\frac{\mathrm{d}p'\left[r'(r)\right]}{\mathrm{d}r'} = \rho_a\cdot\frac{{w_t'}^2\left[r'(r)\right]}{r'(r)} \quad ; \quad p'\left[r'(R)\right] = p_a \qquad \ldots (11)$$

(d) Combining Bernoulli equations for a streamline before it enters the disk and in the wake:

$$\Delta p(r) = p'\left[r'(r)\right] - p_a + \frac{\rho_a}{2}\left\langle\left\{V_F + w_a'\left[r'(r)\right]\right\}^2 - V_F^2 + w_t'\left[r'(r)\right]^2 - w_t(r)^2\right\rangle \qquad \ldots (12)$$

(e) Conservation of axial momentum:

$$\mathrm{d}T(r) = 2\cdot\pi\cdot\rho_a\cdot r'(r)\cdot\left\{V_F + w_a'\left[r'(r)\right]\right\}\cdot w_a'\left[r'(r)\right]\cdot\mathrm{d}r' - 2\cdot\pi\cdot r'(r)\cdot\left\{p_a - p'\left[r'(r)\right]\right\}\cdot\mathrm{d}r' \qquad \ldots (13)$$

(f) Conservation of mass along the control volume:

$$2\cdot\pi\cdot\rho_a\cdot r\cdot\left[V_F + w_a(r)\right]\cdot\mathrm{d}r = 2\cdot\pi\cdot\rho_a\cdot r'(r)\cdot\left\{V_F + w_a'\left[r'(r)\right]\right\}\cdot\mathrm{d}r' \qquad \ldots (14)$$

(g) Conservation of angular momentum — the torque which is applied on the flow through an annulus r, by the actuator disk, is equal to the change in the angular momentum of the flow crossing that annulus:

$$\mathrm{d}Q(r) = 2\cdot\pi\cdot\rho_a\cdot r\cdot\left[V_F + w_a(r)\right]\cdot w_t(r)\cdot r\cdot\mathrm{d}r \qquad \ldots (15)$$

Equations (9)-(15) are seven equations for the following seven unknowns:

(a) Axial and circumferential induced velocity components at the disk plane, $w_a(r)$ and $w_t(r)$.

(b) Axial and circumferential induced velocity components in the far wake, $w'_a[r'(r)]$ and $w'_t[r'(r)]$.

(c) The pressure jump across the disk, $\Delta p(r)$, and the pressure in the far wake, $p'[r'(r)]$.

(d) The radial co-ordinate of the stream line r, in the far wake — $r'(r)$.

It should be noted that the radial induced velocity at the disk plane, $w_r(r)$, does not take part in the general-momentum model. In the case of straight blades this component has no influence on the blade-element's cross-sectional velocities, thus it does not play a roll in the analysis. It can be assumed that the influence of the radial component of the induced velocity can also be neglected in the case of small sweep angles. For higher sweep angles, it is possible to use other models[20] in order to calculate the radial induced velocity, $w_r(r)$, and take into account the influence of its projection onto the blade cross-section, on the blade-element aerodynamic behaviour.

Equations (9)-(15) include two additional unknowns: the thrust and torque which are applied on the flow that passes through the disk's annulus — $\mathrm{d}T(r)$ and $\mathrm{d}Q(r)$, respectively. These unknowns are obtained from Equations (6-7) of the blade-element model.

The combined solution of the blade-element/general-momentum model starts by assuming an initial induced velocity distribution along the blade. Then the thrust and torque distributions along the blades are calculated by using the blade-blement model — Equations (6)-(7). This is followed by calculating the induced velocity using the general-momentum model — Equations (9)-(15) . This scheme is repeated iteratively until convergence. The process converges rapidly and requires relatively small computer resources.

The general-momentum model can be further simplified by adopting the following assumptions:

(a) The pressure in the far wake, $p'[r'(r)]$, is approximately equal to the ambient pressure, p_a:

$$p'\left[r'(r)\right] \cong p_a \quad \forall \quad r' \qquad \ldots (16)$$

(b) The circumferential induced velocity in the far wake is similar to the circumferential induced velocity just after the flow crosses the disk. This approximation leads to the following equation:

$$w_t'\left[r'(r)\right]^2 - w_t(r)^2 \ll \left\{V_F + w_a'\left[r'(r)\right]\right\}^2 - V_F^2 \qquad \ldots (17)$$

After introducing these assumptions into Equations (9)-(15), the system of seven equations is reduced into a system of only two equations, as follows:

$$\mathrm{d}T(r) = 4\cdot\pi\cdot\rho_a\cdot w_a(r)\cdot\left[V_F + w_a(r)\right]\cdot r\cdot\mathrm{d}r \qquad \ldots (18)$$

$$\mathrm{d}Q(r) = 2\cdot\pi\cdot\rho_a\cdot w_t(r)\cdot r\cdot\left[V_F + w_a(r)\right]\cdot r\cdot\mathrm{d}r \qquad \ldots (19)$$

The above approximations also lead to the following well known relation:

$$w_a'\left[r'(r)\right] = 2\cdot w_a(r) \qquad \ldots (20)$$

In many cases Equations (18)-(19) are referred to as 'the momentum model', in the present paper they will be denoted the simplified-momentum model.

One of the assumptions behind an actuator disk model includes an 'averaging' of the phenomenon at any point of the disk. This

https://doi.org/10.1017/S0001924000002669 Published online by Cambridge University Press

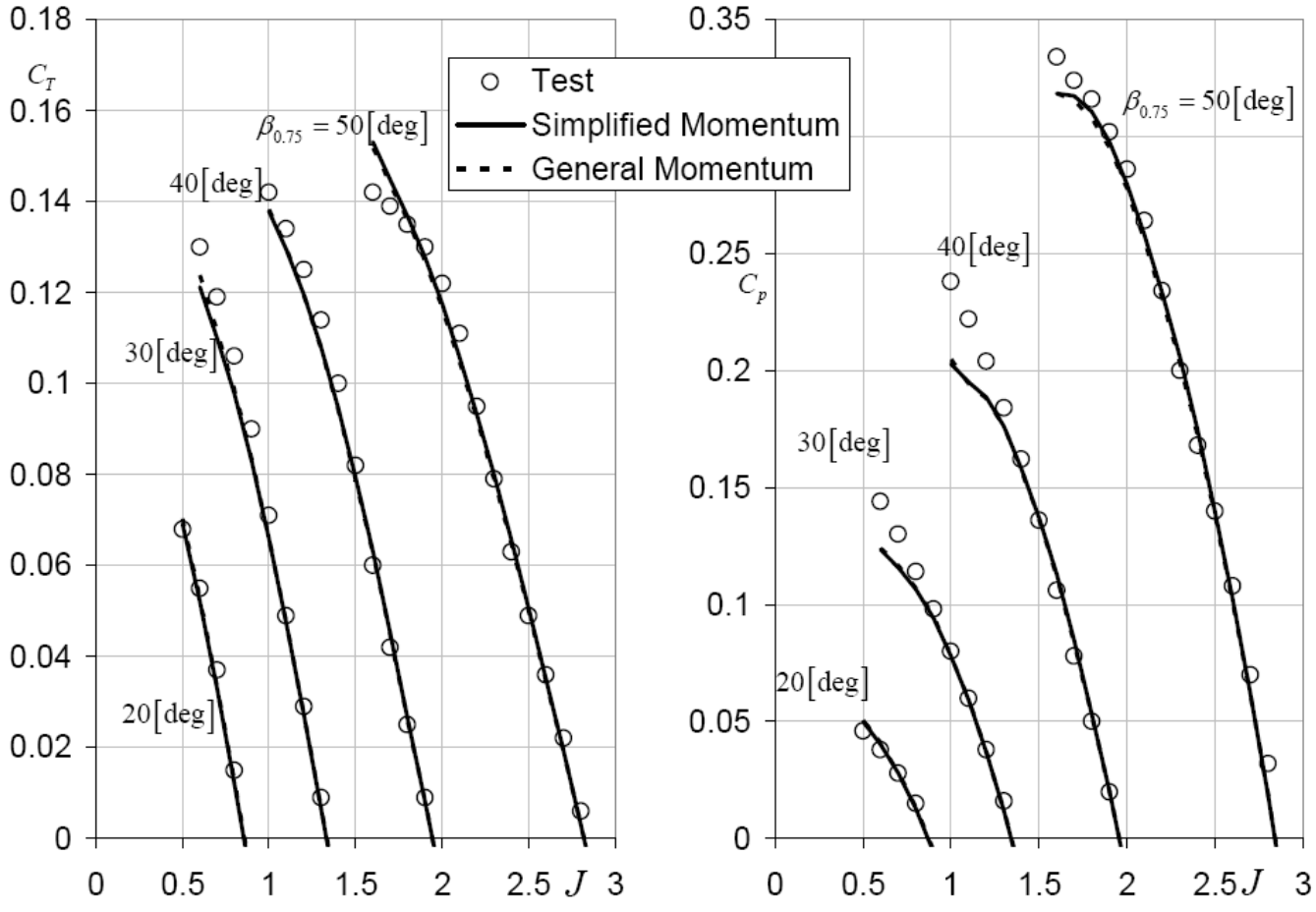


Figure 4. Comparison between the results of momentum models and test results of a two bladed propeller in axial flight (Propeller II of Ref. 22).

averaging is equivalent to 'smearing' the phenomenon, namely assuming that the disk consists of an infinite number of blades. To correct for this assumption, Goldstein's coefficient of interference velocity, $\kappa(r)$, is used[21]. $\kappa(r)$ is a function of the number of blades, N_b, radial co-ordinate, r, and the local inflow angle, $\phi(r)$. It is defined as the ratio between the cross-sectional circulation of a single blade in the case of a finite number of blades, $\Gamma_B(r)$, and the total circulation at that radial co-ordinate, in the case of an infinite number of blades, $\Gamma_B(r)$:

$$\kappa(r) = \frac{N_b \cdot \Gamma_B(r)}{\Gamma_\infty(r)} \quad \ldots (21)$$

This effect is introduced into the momentum model by multiplying the various induced velocity components by $\kappa(r)$. Thus the equations of the simplified-momentum model, Equations (18-19), become:

$$dT(r) = 4 \cdot \pi \cdot \rho_a \cdot r \cdot \left[V_F + \kappa(r) \cdot w_a(r)\right] \cdot \kappa(r) \cdot w_a(r) \cdot dr \quad \ldots (22)$$

$$dQ(r) = 2 \cdot \pi \cdot \rho_a \cdot r \cdot \left[V_F + \kappa(r) \cdot w_a(r)\right] \cdot \kappa(r) \cdot w_t(r) \cdot r \cdot dr \quad \ldots (23)$$

In the same manner $\kappa(r)$ is also introduced into the general-momentum model — Equations (9)-(15).

The circumferential induced velocity before the fluid enters the disk plane is equal to zero. After the flow exits the disk plane the circumferential induced velocity equals w_t. Thus the value of the circumferential induced velocity which is seen by each blade-element, w_{t-BE} (Fig. 1), is somewhere between zero and w_t.
In most cases the average is used:

$$w_{t-BE} = \frac{w_t}{2} \quad \ldots (24)$$

Another approach was suggested by McCormick[11] who introduced a correction to the cross-sectional angle-of-attack, expressing the circumferential induced velocity variation through the disk.

In Fig. 4 the results of the two above described models (general-momentum and simplified-momentum) are compared with test results of a two bladed propeller (propeller II of Ref. 22). This figure shows the thrust and power coefficients, C_T and C_P, respectively, as functions of the propeller advance ratio, J. These parameters are defined as follows:

$$C_T = \frac{T}{\rho_a \cdot n^2 \cdot D^4} \quad \ldots (25)$$

$$C_P = \frac{P}{\rho_a \cdot n^3 \cdot D^5} \quad \ldots (26)$$

$$J = \frac{V_F}{n \cdot D} \quad \ldots (27)$$

https://doi.org/10.1017/S0001924000002669 Published online by Cambridge University Press

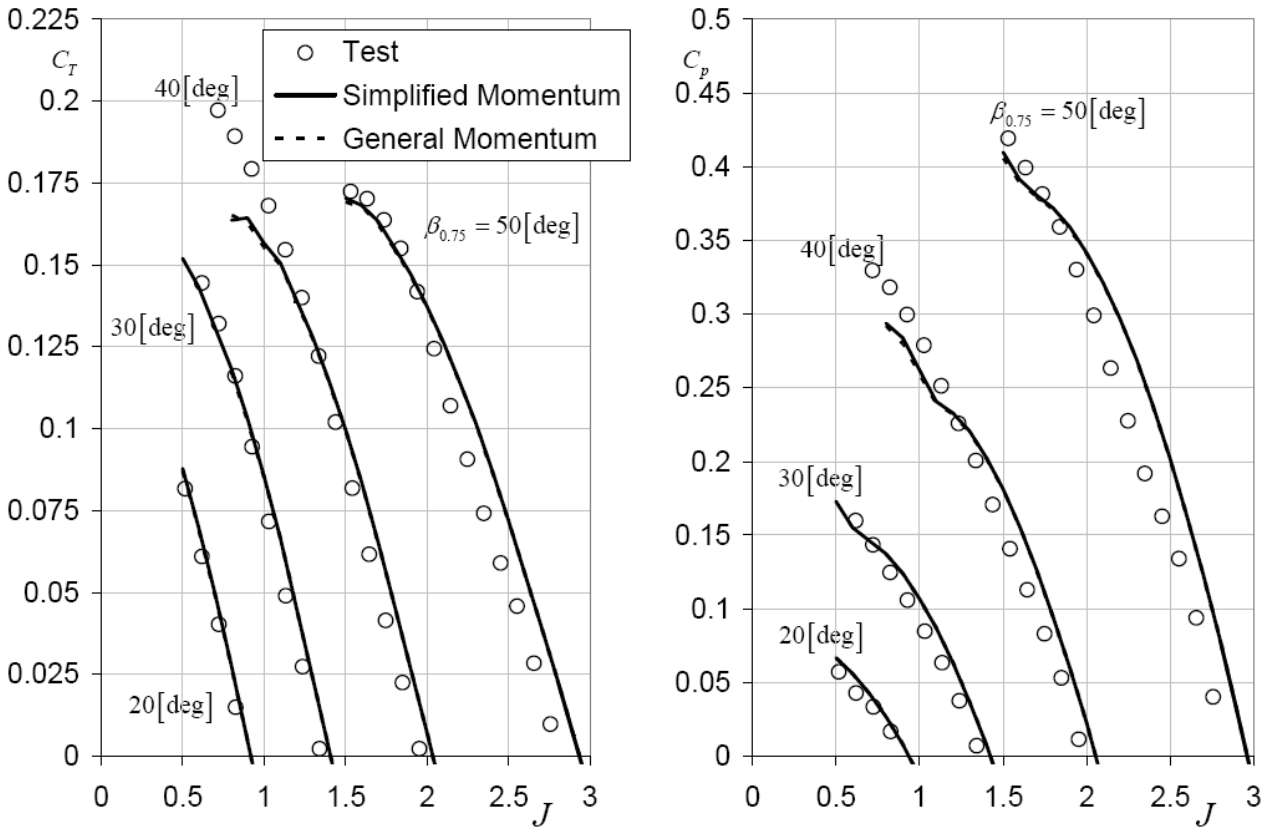


Figure 5. Comparison between the results of momentum models and test results of a propeller having two swept blades, in axial flight (Propeller I of Ref. 22).

T and P are the resultant propeller's thrust and required power, respectively. n is the propeller rotational speed (in revolutions per second) and D is the propeller's diameter. Figure 4 includes results for various pitch angle settings, $\beta_{0.75}$.

According to Fig. 4 the agreement between the calculations and the test results is very good for high advance ratios at each pitch setting. At lower advance ratios, the agreement deteriorates. As mentioned above, at low advance ratio large portions of the blade experience stall and the blade-element model, which is based on two dimensional aerodynamic data, fails to predict the complicated three dimensional stall behavior of these cross-sections[18].

Figure 4 exhibits negligible differences between the results of the general-momentum model and the simplified-momentum model. The computer resources which are needed for the simplified-momentum model are smaller by an order of magnitude compared to the general-momentum model.

In order to further investigate the differences between the general-momentum and simplified-momentum models, a propeller having swept blades is considered. This propeller is identical to propeller I of Ref. 22. In Fig. 5 the test results are compared with calculations, for several pitch angles, $\beta_{0.75}$. Again, there are negligible differences between the general and simplified-momentum models, while both models exhibit good agreement with the experimental results.

Based on the above results, and other comparisons with tests that have not been presented here, it can be concluded that for propeller performance calculations the simplified-momentum model gives good results, exhibiting negligible differences in comparison with results of the general-momentum model.

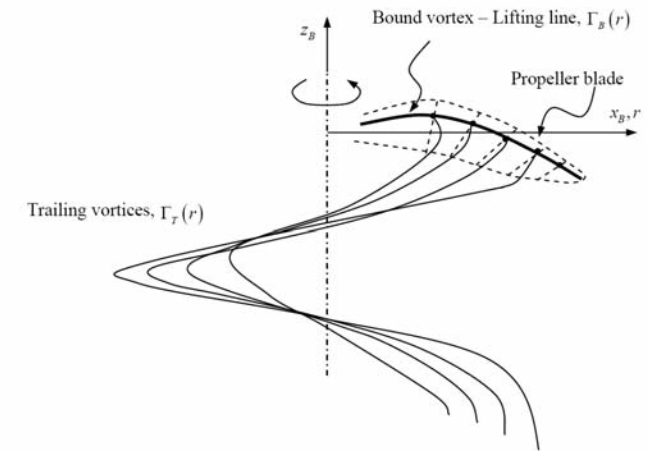


Figure 6. The lifting-line model.

4.0 LIFTING-LINE MODEL

The lifting-line model for fixed wings was developed by Prandtl[13,23] and is still commonly used for various aerodynamic analyses[24].

According to this model, high aspect ratio wings can be represented by a vortex filament which is bound along the wing's quarter chord line (the bound vortex). This bound vortex filament is known as the lifting-line. Due to variations of the circulation along the blade, trailing vortices are created and form the wake.

https://doi.org/10.1017/S0001924000002669 Published online by Cambridge University Press

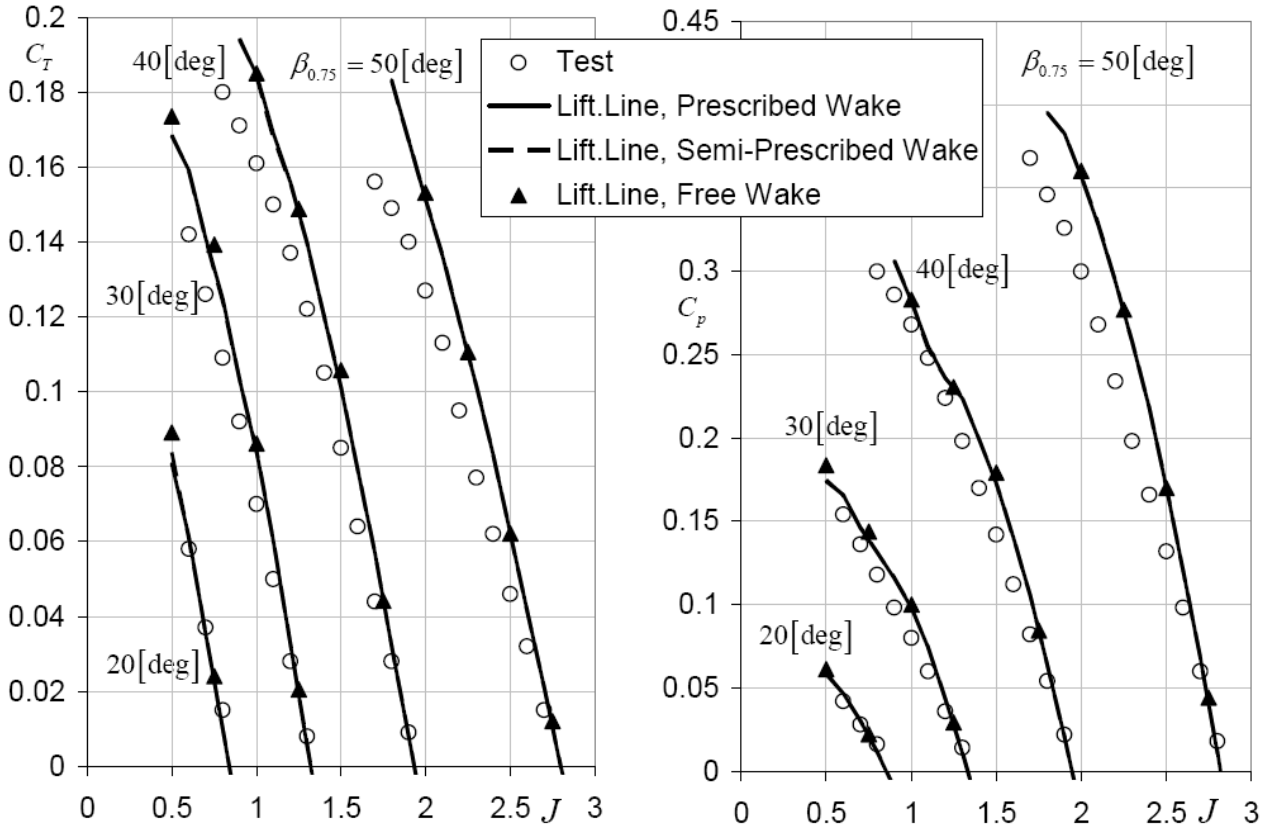


Figure 7. Comparison between the results of lifting-line models and test results of a two bladed propeller in axial flight (Propeller III of Ref. 22).

The lifting-line model was extended by Betz[25] for rotary wings (Fig. 6). By using a lifting-line model Betz defined the conditions for a maximum efficiency propeller. He used a variational approach and after adopting a few assumptions he showed that the vortex sheets in the wake of an optimal propeller move axially backwards as rigid screw surfaces. This result was later used by others, like Goldstein[26] who obtained an expression for the velocity induced by such a wake in the case of lightly loaded propellers, or Theodorsen[10] who extended Goldstein's work to include the case of heavily loaded propellers.

The magnitude of the bound circulation, Γ_B, is a function of the radial co-ordinate r. The circulation magnitude of the trailing vortex filaments per unit spanwise length, Γ_T, is calculated based on the law of conservation of circulation:

$$\Gamma_T(r) = \frac{d\Gamma_B(r)}{dl_B} \quad \ldots (28)$$

l_B is the co-ordinate along the blade's quarter chord.

If the trajectories of the trailing vortices are known, namely the wake geometry is known, one can calculate the induced velocity at any point of the flow field.

The direction of the trailing vortices at any point of the field coincides with the direction of the local resultant velocity[14], thus the trailing vortices are free of forces. The free wake model is based on this condition. This model is quite complicated and requires relatively large computer resources. By using this method the actual geometry of the wake is calculated. Such a calculation is especially important for static conditions[27], where the wake geometry is fairly complicated, showing a significant contraction.

Instead of finding the free wake geometry as discussed above, it is possible to adopt simplifying assumptions that define the entire wake geometry based on certain parameters. These models are known as prescribed wake models. In the case of propellers it is common to assume that each vortex filament in the wake has a helical geometry with a constant radius and pitch. The radius is equal to the radial location of the origin of the trailing vortex filament at the disk plane. Regarding the pitch, $p_Z(r)$, two common approaches are used:

(a) The induced velocity is neglected compared to the flight velocity, V_F, and the tangential blades' velocity, $\Omega \cdot r$. Thus the wake's pitch becomes:

$$P_Z(r) = 2 \cdot \pi \cdot \frac{V_F}{\Omega} \quad \ldots (29)$$

According to this model the wake geometry is defined *a priori* and it does not change throughout the entire iterative solution process. This model is denoted a (fully) prescribed wake model.

(b) The influence of the axial component of the induced velocity on the helical pitch is taken into account. Thus the helix pitch is given by the following expression:

$$P_Z(r) = 2 \cdot \pi \cdot \frac{V_F + w_{a-Wake}(r)}{\Omega} \quad \ldots (30)$$

$w_{a-Wake}(r)$ is the axial induced velocity in the wake. The magnitude of this velocity lies between the disk axial induced velocity, $w_a(r)$, and the far wake velocity, $w'_a[r'(r)]$. According to numerical investigations, the differences between the results

https://doi.org/10.1017/S0001924000002669 Published online by Cambridge University Press

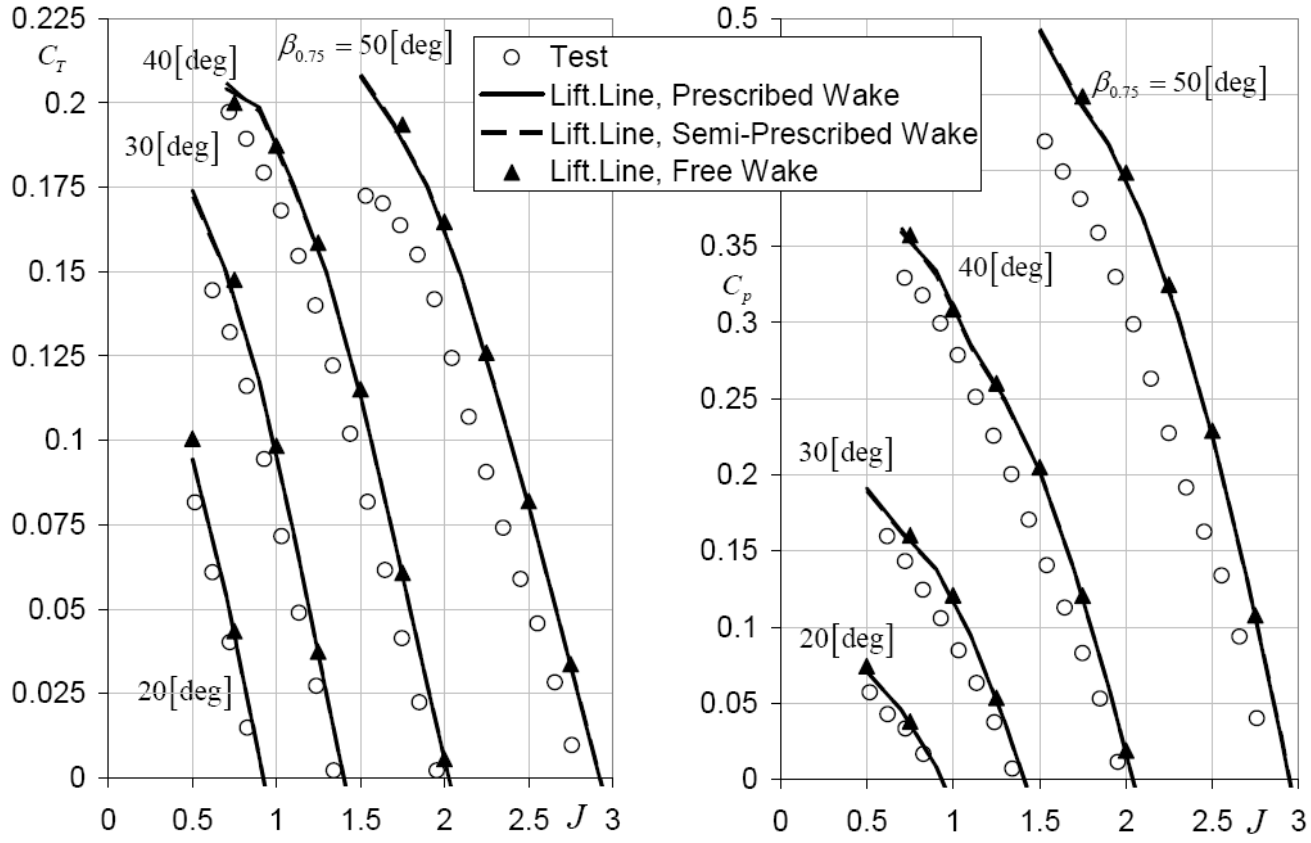


Figure 8. Comparison between the results of lifting-line models and test results of a propeller having two swept blades, in axial flight (Propeller I of Ref. 22).

while using these two values are very small.

Since the induced velocity (including its axial component) is a function of the wake geometry, an iterative solution procedure is required. Thus this method is denoted a semi-prescribed wake model.

It is clear that the prescribed wake model is simpler and more efficient than the semi-prescribed wake model. This model can become even more efficient by using semi-analytical methods to calculate the velocities induced by helical vortex filaments[28]. Nevertheless, in certain cases it is necessary to use free wake or the semi-prescribed wake models in order to obtain good results. For example, during static operation of propellers or for hovering rotors, a free wake model should be used since the free stream velocity is equal to zero. However investigation of the static thrust case was beyond the scope of the present work.

After the wake geometry has been defined by using one of the above described models, it is necessary to combine the lifting-line with the blade-element model. The induced velocity along the bound vortex is calculated by using the Biot-Savart law. In certain cases more complex models, rather than the simple Biot-Savart, are used, including modeling of the vortex core[29]. The induced velocities that are calculated using these methods, are projected onto the blade-element cross-section.

Figures 7 and 8 present comparisons between the results of lifting-line models and test results of a propeller with straight blades (propeller III of Ref. 22) and a propeller with swept blades (propeller I of Ref. 22). Results of three lifting-line models are shown:

(a) A prescribed wake model

(b) A semi-prescribed wake model

(c) A free wake model

The differences between the three lifting-line models are negligible and the agreement with the experimental results is good in general, except for swept blades at high pitch angles (possible reasons for that are discussed in Section 6).

For lifting-line models, as in the two versions of the momentum model (general and simplified), the small differences between the various lifting-line models do not justify the use of the more complex ones, namely the free or semi-prescribed wake models, for the analysis of propellers at typical operating conditions.

5.0 VORTEX MODELS

Vortex models represent another method of calculating the induced velocities along the blades. Here Theodorsen's[10] and McCormick's[11] models will be discussed. These two models are similar and are based on the same assumptions. Originally they were developed for straight blades in axial flight, but they can be extended to include moderately swept blades[19].

According to Betz the vortex sheets in the wake of an optimal propeller move axially backward as rigid screw surfaces. In this case[10,11,21,30] the resultant velocity of the vortex sheets is normal to the vortex surfaces, namely the resultant induced velocity in the far wake is normal to the resultant velocity there. Theodorsen[10] and

https://doi.org/10.1017/S0001924000002669 Published online by Cambridge University Press

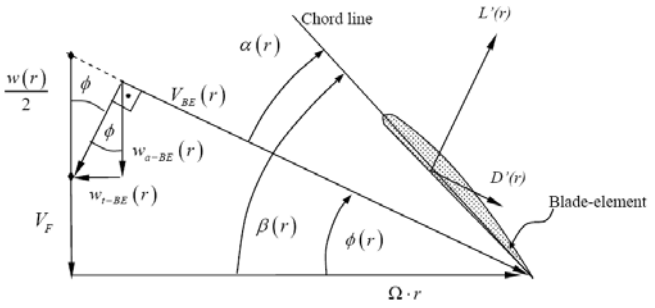


Figure 9. Cross-sectional velocities of the vortex model.

later McCormick[11] went further and assumed that at the disk plane the cross-sectional resultant induced velocity is also perpendicular to the resultant velocity (Fig. 9)

It is now convenient to define the displacement velocity in the far wake, w, It was shown previously, based on the momentum model and certain assumptions, that the magnitude of the induced velocity in the disk plane is half its magnitude in the far wake — Equations (20) and (24). Therefore at the disk plane the magnitude of the displacement velocity is assumed to be half its value in the far wake. Knowing the displacement velocity (and from it the inflow angle, ϕ) allows the calculation of the axial and circumferential components of the induced velocity.

5.1 Theodorsen's model

Theodorsen's model is based on the earlier work of Goldstein[26]. The main results of Theodorsen appear in the following expression for the displacement velocity, w .

$$\left[V_F + w(r)\right]\cdot w(r) = \frac{1}{2}\cdot\frac{V_{BE}(r)\cdot\sigma(r)\cdot\Omega\cdot r\cdot\tilde{C}_l(r)}{K\left(N_b,\lambda,r/R\right)} \quad \ldots (31)$$

$\sigma(r)$ is the local solidity:

$$\sigma(r) = \frac{N_b\cdot c(r)}{2\cdot\pi\cdot r} \quad \ldots (32)$$

Equation (31) presents a relation between the blade aerodynamic loading (the distribution of the lift coefficient) that is obtained from the blade-element model, and the displacement velocity. The origin of this expression is the Kutta-Joukowski theorem that relates between the magnitude of the local circulation and the local lift force.

K is Theodorsen's circulation function which is a function of: the number of blades, N_b, radial location of the blade-element, r/R, and the advance ratio in the far wake, λ (the tangent of the pitch angle in the far wake).

λ is calculated by using the wake contraction coefficient, Y:

$$\lambda = \frac{V_F}{\Omega\cdot r}\cdot\left(1+\frac{w}{V_F}\right)\cdot\left(1+2\cdot\frac{w}{V_F}\cdot Y\right) \quad \ldots (33)$$

Tabulated values for Y are given in the literature[31].

There is a relation between K and Goldstein's coefficient of interference velocity, κ, which is given by the following equation[21]:

$$\kappa = K\cdot\left[1+\left(\frac{\lambda}{R/r}\right)^2\right] \quad \ldots (34)$$

For lightly loaded propellers the pitch angle is constant along the wake, thus λ is approximately equal to the tangent of the inflow angle at the disk plane, ϕ:

$$\lambda \cong \mathrm{Tan}\phi \quad \ldots (35)$$

Goldstein's derivation dealt with lightly loaded propellers where the displacement velocity has a negligible influence on the inflow angle in the disk plane and in the far wake.

According to Theodorsen's model, the displacement velocity is calculated by using geometrical relations (Fig. 9) between the inflow angle, axial and circumferential induced velocities:

$$\mathrm{Tan}\phi = \frac{v_F}{\Omega\cdot r}\cdot\left(1+\frac{w}{2\cdot V_F}\right) \quad \ldots (36)$$

$$w_{a-BE} = \frac{w}{2}\cdot\mathrm{Cos}^2\phi \quad \ldots (37)$$

$$w_{t-BE} = \frac{w}{2}\cdot\mathrm{Cos}\phi\cdot\mathrm{Sin}\phi \quad \ldots (38)$$

5.2 McCormick's model

McCormick's model is similar to Theodorsen's model and includes the following expression for the circumferential induced velocity, $w_{t-BE}(r)$[11]:

$$w_{t-BE}(r) = \frac{\sigma(r)\cdot V_{BE}(r)\cdot\tilde{C}_l(r)}{2\cdot\kappa(r)} \quad \ldots (39)$$

By using Fig. 9 the following geometrical relation for the axial induced velocity is obtained:

$$w_{a-BE}(r) = -\frac{1}{2}\cdot V_F + \sqrt{\left(\frac{V_F}{2}\right)^2 + w_{t-BE}(r)\cdot\left[\Omega\cdot r - w_{t-BE}(r)\right]} \quad \ldots (40)$$

It is possible to obtain the aerodynamic loads along the blade by using Equations (39) and (40), together with the blade-element model.

6.0 COMPARISON BETWEEN THE DIFFERENT MODELS

In the previous sections a few of the common blade-element based models of propellers were described: momentum models, lifting-line models, and vortex models. As for the momentum and lifting-line models, their main versions were presented and the results showed that for propellers in axial flight the differences between the various versions are negligible. Thus the simplified-momentum model and lifting-line with prescribed wake, which are simpler and require smaller computer resources, will be considered in what follows.

Figures 10-12 present comparisons between the four models and test results[22,32] of three propellers with straight blades in axial flight. Figure 13 presents the efficiency, η, of the propeller presented in Fig. 12. Figure 14 shows a similar comparison for the propeller with swept blades[22]. It should be noted that the propeller of Ref. 32 reaches higher advance ratios and thus it increases the range of comparisons.

In all the cases the results of McCormick's model give the lowest values. Theodorsen's model over predicts the values, in comparison with the test results, and agrees with the much more complicated lifting-line model. The momentum model lies in between these models.

As the pitch angle increases, the differences between the results of the various models increase. This is due to the increase of the thrust

https://doi.org/10.1017/S0001924000002669 Published online by Cambridge University Press

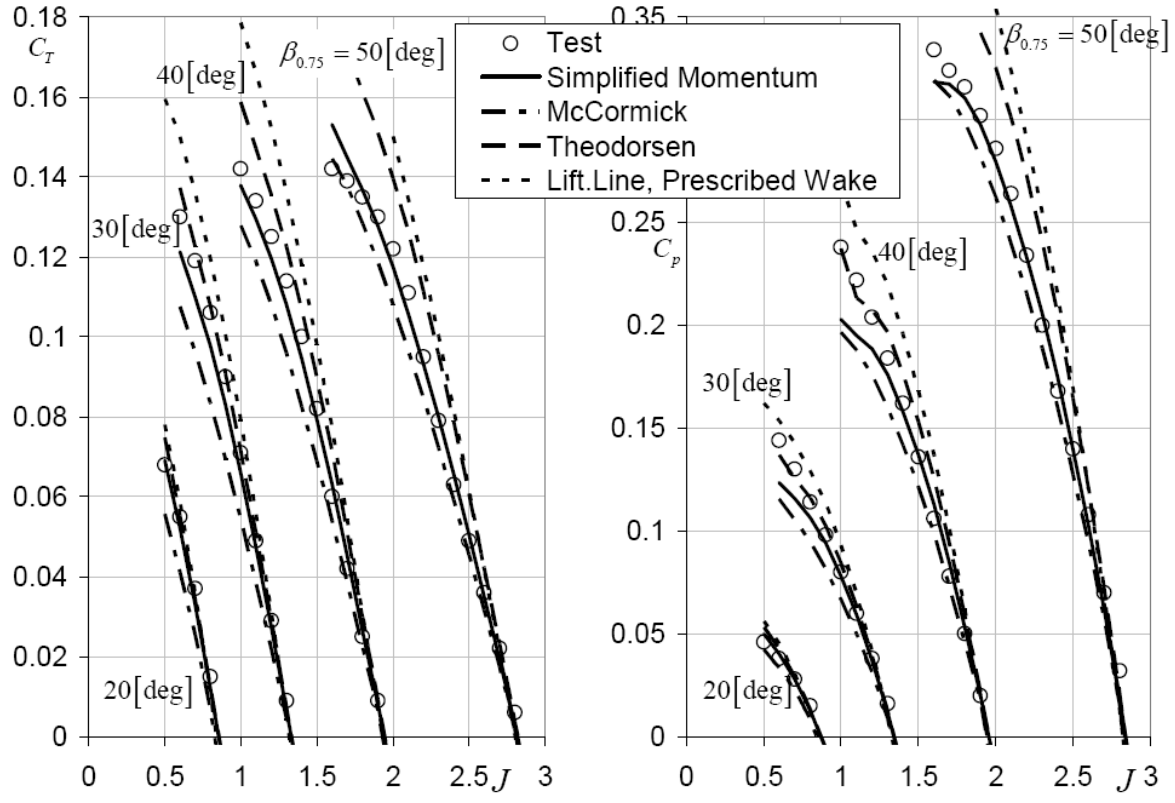


Figure 10. Comparison between the various models and test results of a two bladed propeller in axial flight (Propeller II of Ref. 22).

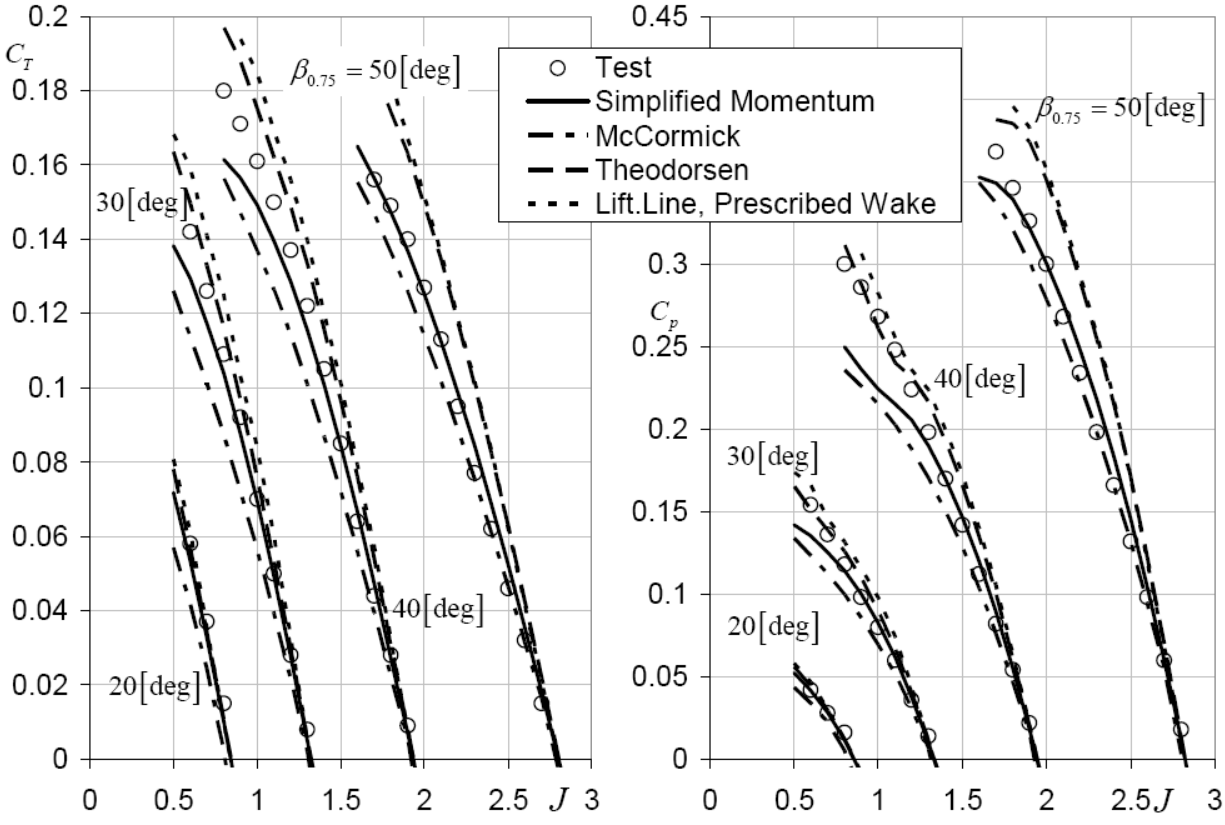


Figure 11. Comparison between the various models and test results of a two bladed propeller in axial flight (Propeller III of Ref. 22).

https://doi.org/10.1017/S0001924000002669 Published online by Cambridge University Press

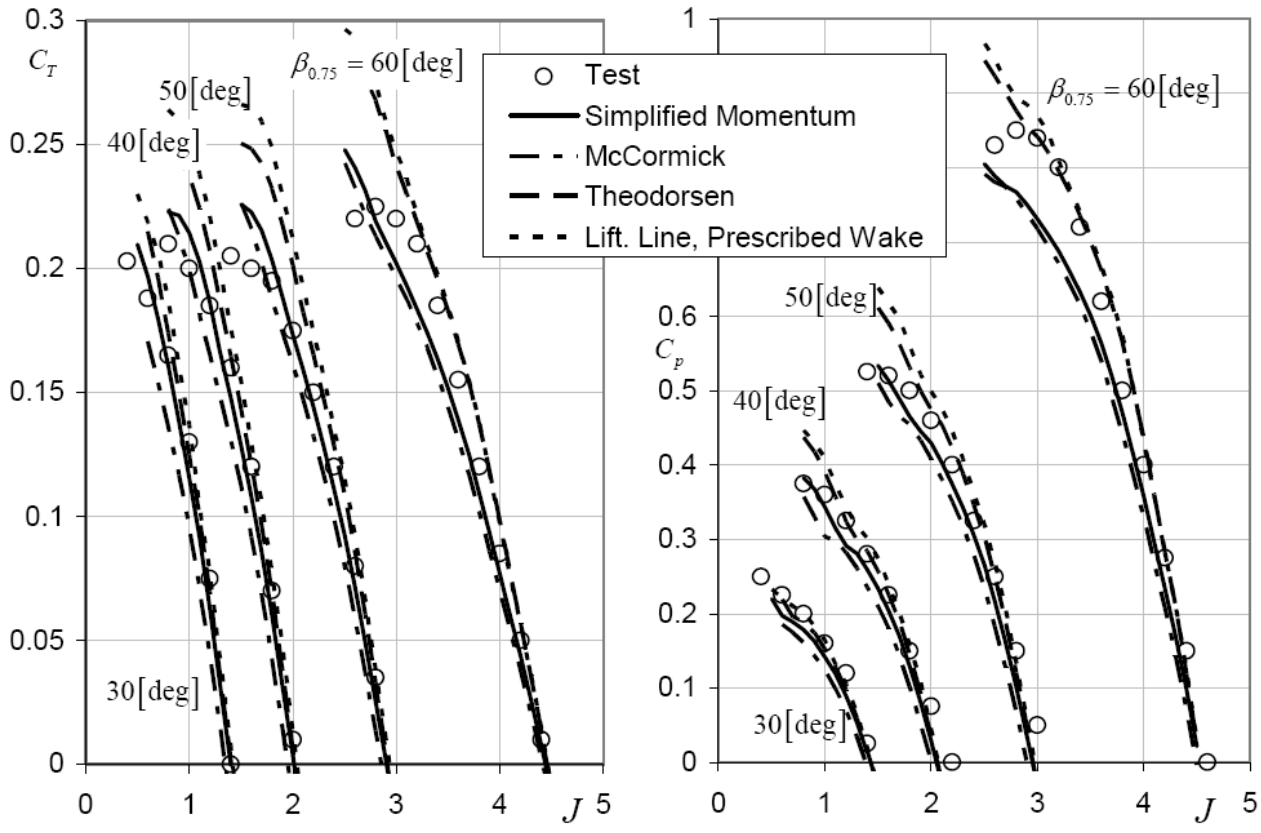


Figure 12. Comparison between the various models and test results of a four bladed propeller in axial flight (Ref. 32).

and power that result in an increase of the induced velocities and consequently an increase of their influence on the results. In a similar manner, at low flight velocities the thrust and power increase and again the induced velocities become more important. Thus, as the advance ratio decreases the differences between the results of various models increase.

Propeller's efficiency is defined as follows:

$$\eta = \frac{J \cdot C_T}{C_P} \qquad \ldots (41)$$

According to Fig. 13 McCormick's model under predicts the test results, the lifting-line and Theodorsen's models over predicts them, while the momentum model falls in between.

For swept blades (Fig. 14), as the pitch angle and advance ratio increase, most of the models over predict the test results. The elastic torsion of the swept blades, as a result of the increased torsional moment due to sweep, result in a smaller effective pitch angle in the test, which may be the reason, at least partially, for the over prediction of the theoretical results. The only model that exhibits a fair agreement with the test results, at high advance ratios, is McCormick's model that exhibits under prediction in the case of straight blades.

A more detailed comparison between the different models is presented in Figs 15-19. For propeller II of Ref. 22, at two different advance ratios (J = 1·2 and J = 1·7), the distributions along the blade of the following parameters are presented:

(a) thrust coefficient, $dC_T/d(r/R)$

(b) power coefficient, $dC_p/d(r/R)$

(c) normalised axial induced velocity, $w_a/\Omega R$

(d) normalised circumferential induced velocity, $w_t/\Omega R$

(e) angle-of-attack, α

As expected, at advance ratio J = 1·2 the thrust and power coefficients are higher than at J = 1·7. The differences between the maximal values of the thrust and power distributions in Figs 15 and 16 agree with the differences between the total thrust and power coefficient as presented in the previous comparisons: Theodorsen's and the lifting-line models give the higher values, McCormick's model gives lower values, while the simplified momentum model lies in between. All the distributions exhibit the same behaviour

In contrary to the results presented in Figs 15 and 16 (Theodorsen's and lifting-line models give similar results, while McCormick's results are significantly different, and the momentum results are in between), in Fig. 17 except for the results of McCormick's model, all the other models give very close results. The circumferential induced velocity, which is presented in Fig. 18, shows different trends: while the results of Theodorsen's and lifting-line models are similar, McCormick's model give much higher values while those of the momentum model are even higher.

The angle-of-attack is shown in Fig. 19. The trends here agree very nicely with the trends in Figs 15 and 16. Thus the results for Figs 15-19 indicate that, in contrast to other rotary wings (for example helicopter rotors), the influence of the circumferential induced velocity on the blade-element calculations is not negligible and it cannot be neglected compared to the circumferential velocity due to rotation, $\Omega \cdot r$.

https://doi.org/10.1017/S0001924000002669 Published online by Cambridge University Press

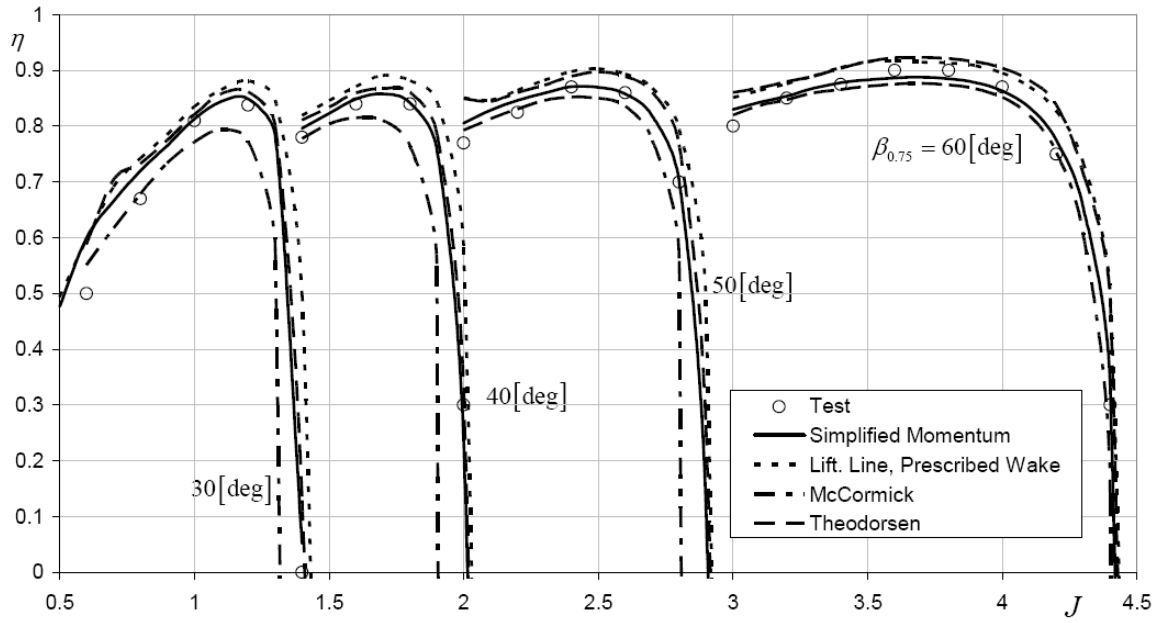


Figure 13. Comparison between the various models and test results of a two bladed propeller in axial flight (Ref. 32).

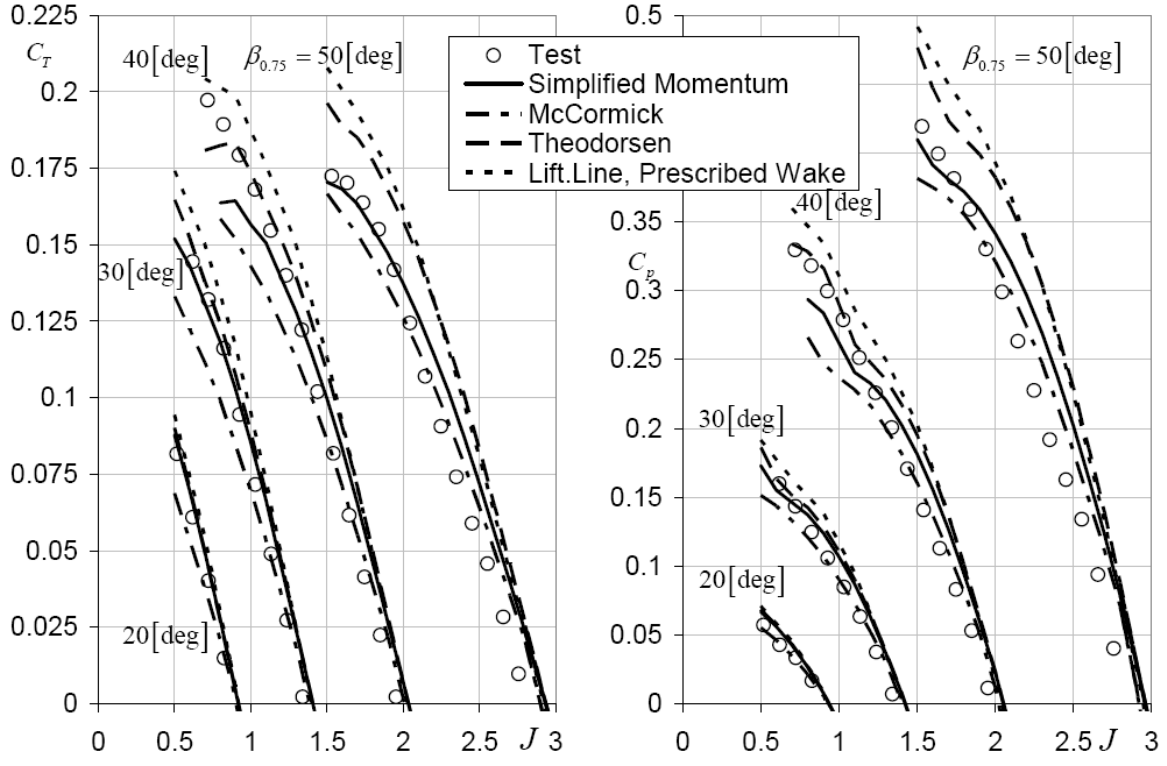


Figure 14. Comparison between the various models and test results of a propeller having two swept blades, in axial flight (Propeller I of Ref. 22).

7.0 CONCLUSIONS

A few of the most common blade-element based models were investigated: momentum models, lifting-line models, and vortex models (McCormick and Theodorsen). In the case of momentum models, the general-momentum and simplified-momentum models were discussed. For forward flight of propellers, the differences between the results of these two models are negligible. Three lifting-line models that differ in their wake geometry modeling were investigated: prescribed, semi-prescribed, and free wake models. Similar to the to momentum models, the differences between the results of these three models are negligible for the case of a propeller in forward flight.

https://doi.org/10.1017/S0001924000002669 Published online by Cambridge University Press

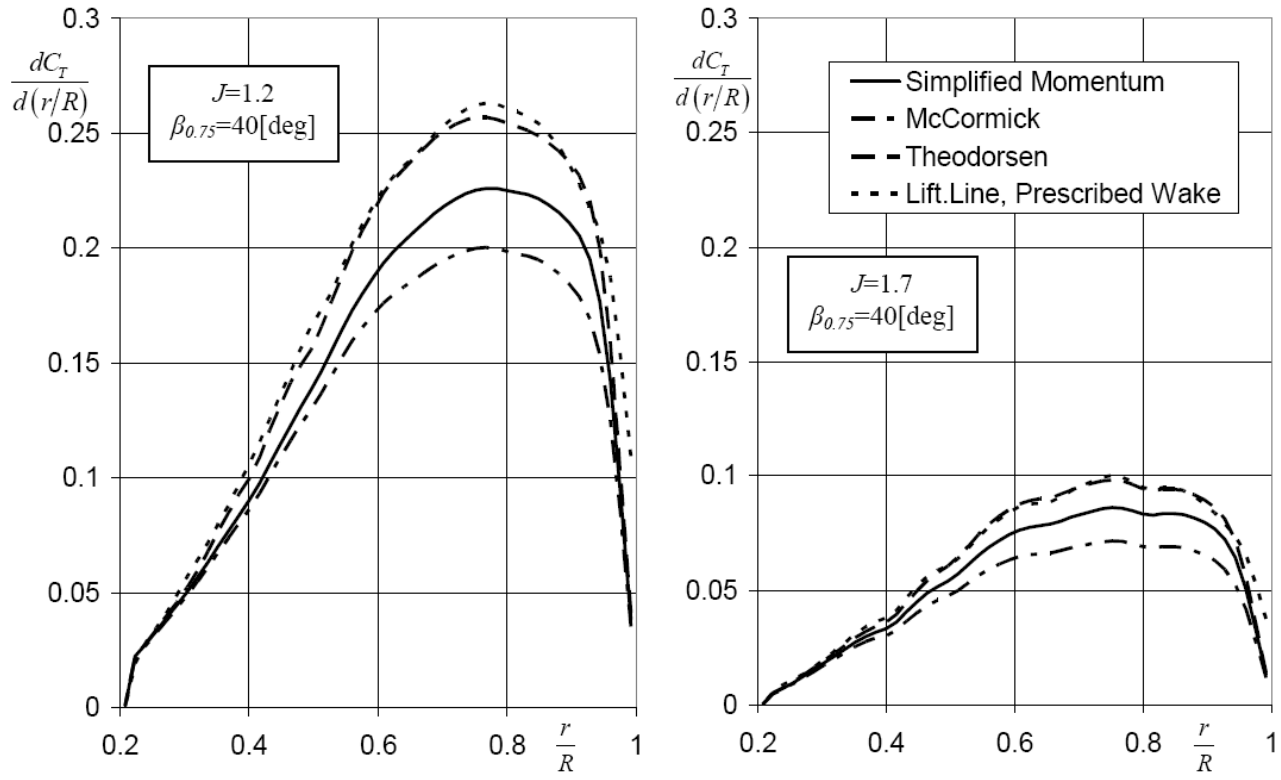


Figure 15. Comparison between the various models of the thrust coefficient distribution of a two bladed propeller in axial flight (Propeller II of Ref. 22).

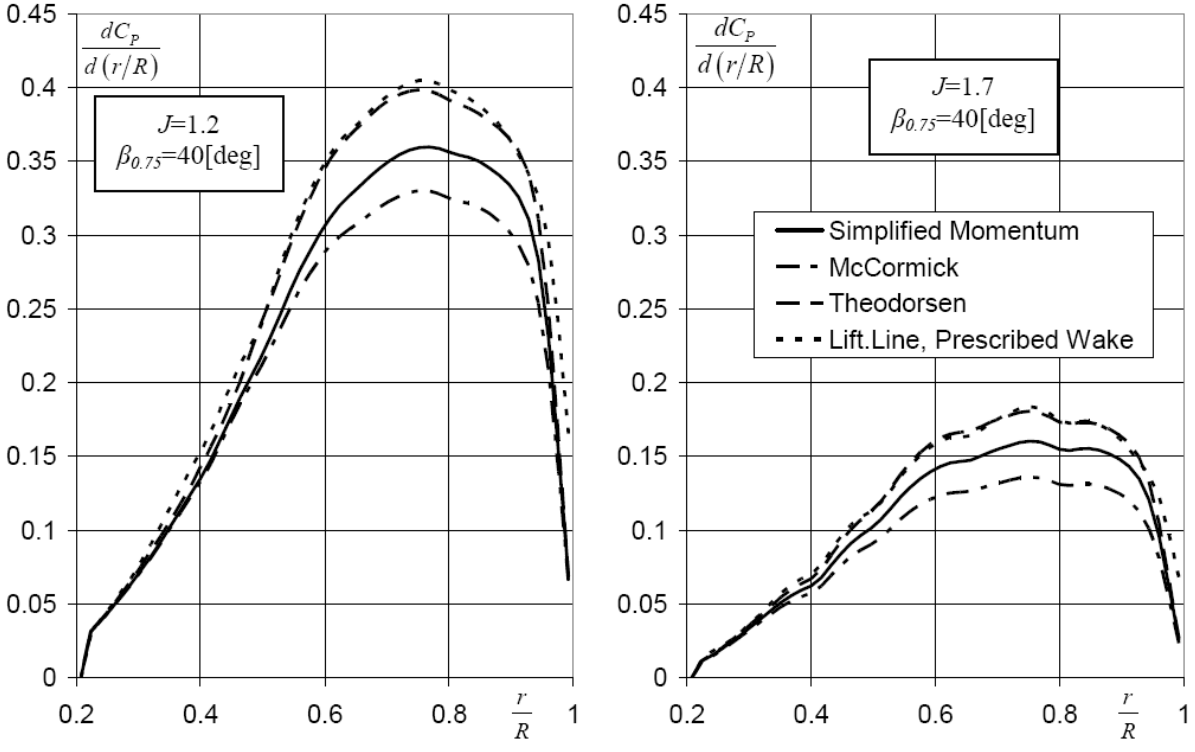


Figure 16. Comparison between the various models of the power coefficient distribution of a two bladed propeller in axial flight (Propeller II of Ref. 22).

https://doi.org/10.1017/S0001924000002669 Published online by Cambridge University Press

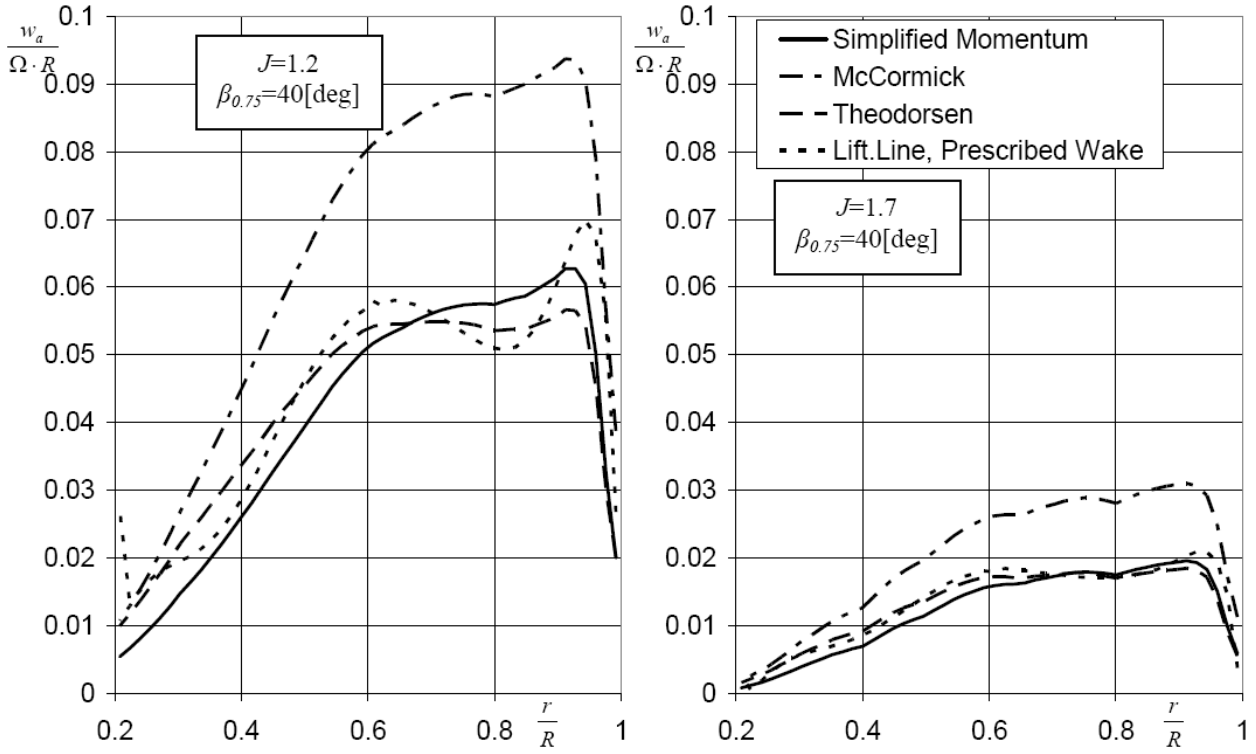


Figure 17. Comparison between the various models of the axial induced velocity distribution of a two bladed propeller in axial flight (Propeller II of Ref. 22).

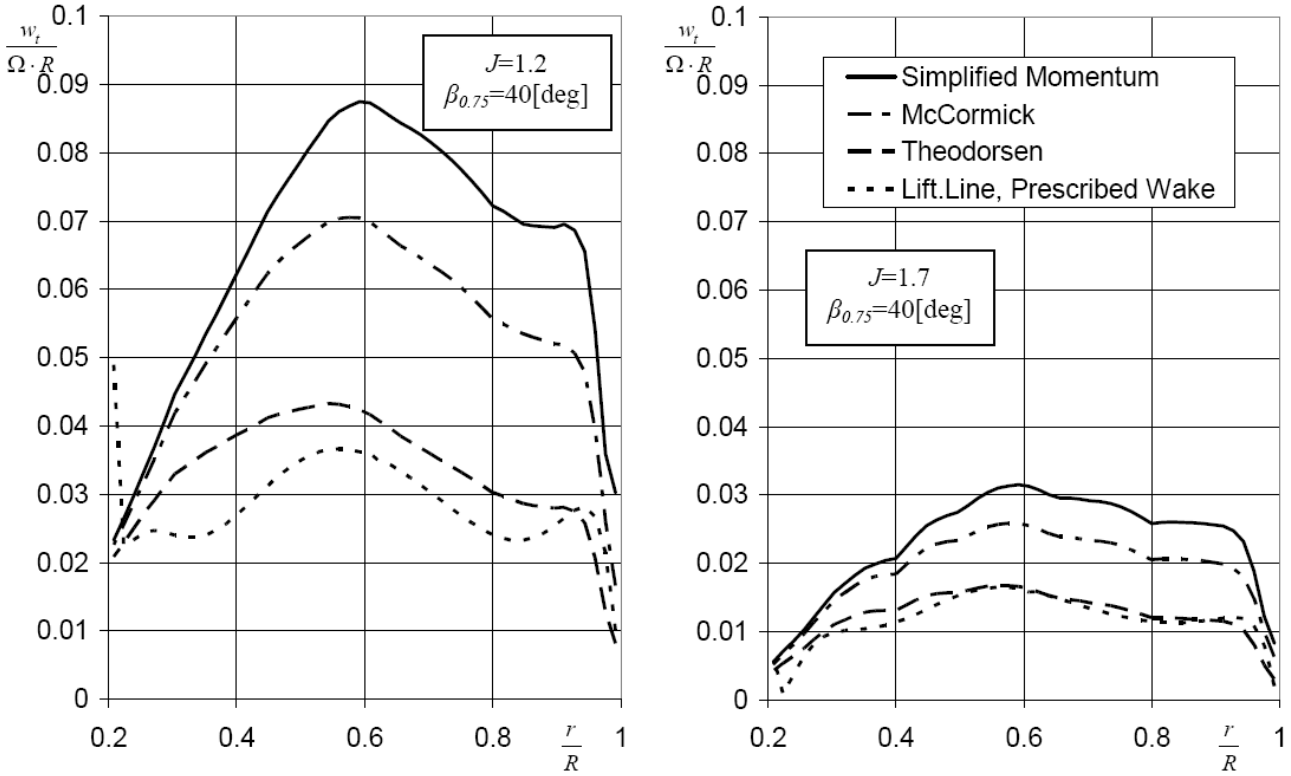


Figure 18. Comparison between the various models of the circumferential induced velocity distribution of a two bladed propeller in axial flight (Propeller II of Ref. 22).

https://doi.org/10.1017/S0001924000002669 Published online by Cambridge University Press

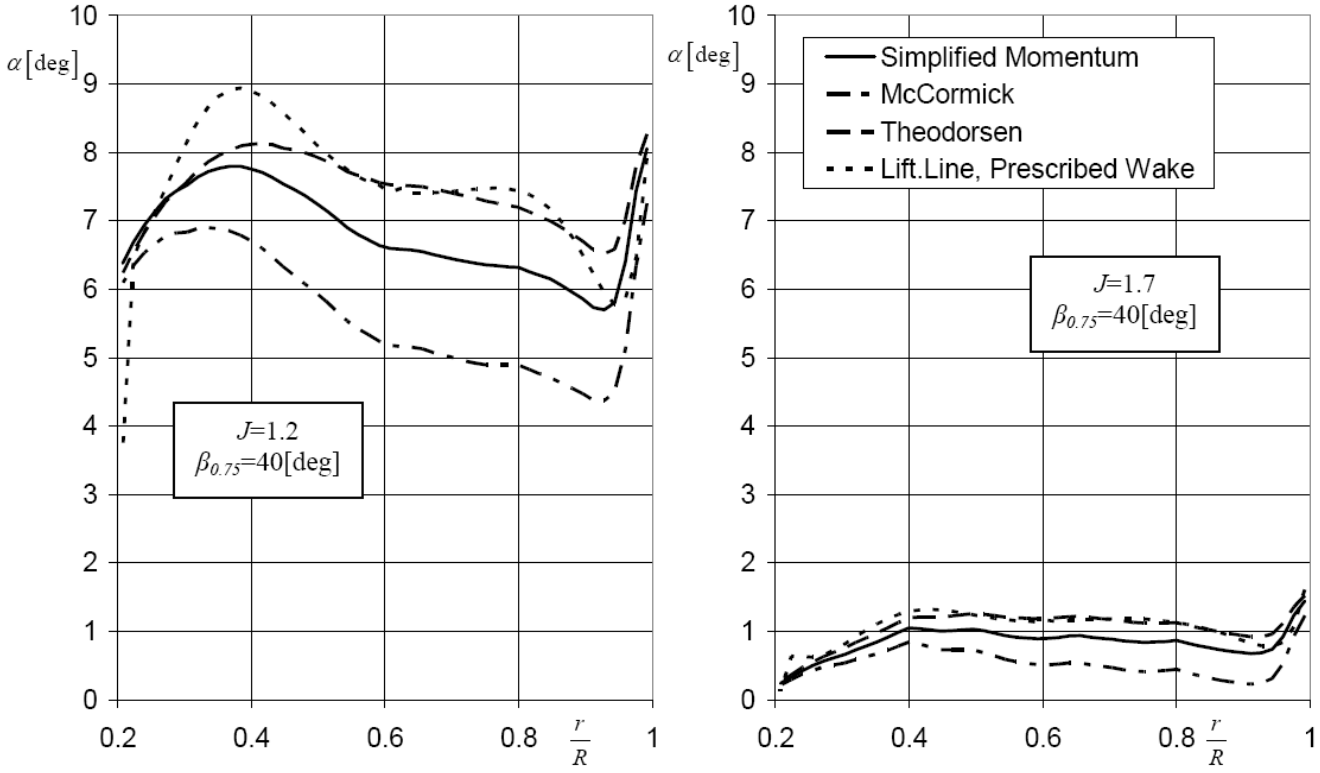


Figure 19. Comparison between the various models of the angle of attack distribution of a two bladed propeller in axial flight (Propeller II of Ref. 22).

For the case of axial flight of propellers having straight blades or having small sweep angles, it is recommended, due to the low demand of computer resources, to use the simpler model, namely the simplified-momentum model. Although this model is very simple and thus very efficient, it gives results of reasonably high quality, depending on conditions.

Larger differences between the various models appear at high thrust and low advance ratios or static operation. At these flight conditions the magnitude of the induced velocity increases. This increases the influence of the induced velocity on the propeller's performance. During static operation it is important to use more accurate models, such as the lifting line free wake model with nonlinear aerofoil aerodynamics, in order to calculate the wake geometry and thus obtain good results.

Comparison between the results of the various models and test results show that the agreement of blade-element based models with the test results is good. The lifting-line models and Theodorsen's model seem to over predict the thrust and required power. On the other hand, McCormick's model under predicts the test results. The momentum models lies in between and generally shows very good agreement with the test results. For propellers with swept blades it seems that because of the elastic deformations of the propeller's blade, especially the elastic torsion, most of the models over predict the test results when elastic torsion is not taken into account.

It should be noted that the differences between the various models, for a certain pitch angle ($\beta_{0.75}$) and advance ratio (J), are not necessarily small and in many cases exceed 20%. Yet, small variations of the advance ratio (meaning small variation of the flight speed or propeller angular speed), or small variations of the pitch angle, result in variations in the aerodynamic loads and propeller's performance that are of the same order of magnitude as the differences between the various models.

REFERENCES

1. SEZER-UZOL, N. and LONG, N.L. 3-D time accurate CFD simulations of wind turbine rotor flow fields, 2006, AIAA Paper 2006-394, 44th AIAA Aerospace Sciences Meeting and Exhibition, 9-12 January 2006, Reno, Nevada.
2. JANUS, J.M. General aviation propeller-airframe integration simulations, *AIAA J Aircr*, March-April 2006, **43**, (2), pp 390-394.
3. KOBAYAKAWA, M. and HATANO, I. Flow field around a propeller by Navier-Stokes equation analysis, AIAA Paper 88-3150, AIAA/ASME/SAE/ASEE 24th Joint Propulsion Conference, 11-13 July 1988, Boston, Massachusetts.
4. YOON, S.J. and SCHETZ, J.A. Numerical Navier-Stokes solutions of high-speed propeller flows, *AIAA J Propulsion*, July-August 1988, **4**, (4), pp 291-292.
5. WALD, Q.R. The Wright brothers propeller theory and design, 2001, AIAA Paper 2001-3386, AIAA/ASME/SAE/ASEE 37th Joint Propulsion Conference and Exhibition, 8-11 July 2001, Salt Lake City, Utah.
6. DRZEWIECKI, S. *Théorie Générale de L'hélice*, 1920, Paris.
7. HUNSAKER, F.D. A numerical blade element approach to estimating propeller flowfields, 2007, AIAA Paper 2007-374, 45th AIAA Aerospace science Meeting and Exhibition, 8-11 January 2007.
8. GLAUERT, H. Airplane propellers, *Aerodynamic Theory*, , 1935, Third Edition, Vol 4, Division L, DURAND, F.W. (Ed), Dover, New York.
9. CLARK, R.D. and LEIPER, C.A. The free wake analysis. A method for the prediction of helicopter rotor hovering performance, *J American Helicopter Soc*, 1970, **15**, (1), pp 3-11.
10. THEODORSEN, T. *Theory of Propellers*, 1948, McGraw-Hill Book Company.
11. MCCORMICK, B.W. *Aerodynamics of V/STOL Flight*, 1967, Academic Press, New-York.
12. HORLOCK, J.H. *Actuator Disk Theory*, 1978, McGraw-Hill.
13. PRANDTL, L. Application of modern hydrodynamics to aeronautics, 1923, NACA Technical Report No 116.

https://doi.org/10.1017/S0001924000002669 Published online by Cambridge University Press

14. BOBER, L.J. and MITCHELL, G.A. Summary of advanced methods for predicting high speed propeller performance, 1980, AIAA Paper 80-0225, 18th Aerospace Sciences Meeting, 14-16 January 1980, Pasadena, California.
15. LOCK, C.N.H. and BATEMAN, H. Experiments with a family of airscrew. Part III: Analysis of the family of airscrew by means of the vortex theory and measurements of total head, December 1923, Aeronautical Research Committee, Report & Memoranda No 892.
16. SHEN, W.Z., SORENSEN, J.N. and MIKKELSEN, R. Tip loss correction for actuator/Navier-Stokes computations, *J Solar Energy Engineering*, May 2005, **127**, pp 209-213.
17. SISSINGH, G. Contribution to the aerodynamic of rotating-wing aircraft, December 1939, NACA Technical Memorandums No 921.
18. GUR, O. and ROSEN, A. Propeller performance at low advance ratio, *AIAA J Aircr*, March-April 2005, **42**, (2), pp 435-441.
19. SANDAK, Y. and ROSEN, A. Aeroelastically adaptive propeller using blade;s root flexibility, *Aeronaut J*, August 2004, **108**, (1086), pp 411-418.
20. ROSEN, A. and GUR, O. A novel approach to actuator disk modeling, 2006, 32nd European Rotorcraft Forum, 12-14 September 2006, Maastricht, The Netherlands.
21. WALD, Q.R. The aerodynamics of propellers, *Progress in Aerospace Sciences*, 2006, **42**, pp 85-128.
22. EVANS, J.A. and LINER, G. A wind tunnel investigation of the aerodynamic characteristics of a full-scale sweptback propeller and two related straight propellers, January 1951, NACA Research and Memorandum L50J05.
23. KARAMCHETI K. *Principles of Ideal-Fluid Aerodynamics*,1980, Krieger Publishing Company.
24. WICKENHEISER, A. and GARCIA, E. Aerodynamic modeling of morphing wings using an extended Lifting-Line analysis, *J Aircr*, January-February 2007, **44**, (1), pp 10-16.
25. BETZ, A. Screw propeller with minimum energy loss (Schraubenpropeller mit geringstem energieverlust), 1919, Translation from German by SINCLAIR, D.A. Translation Section, NRC Library, Technical translation 736, Source: Nachr Kgl Ges Wiss Göttingen, *Math-Phys Kl*, 1919, **2**, pp 193-217.
26. GOLDSTEIN, S. On the vortex theory of screw propellers, Proceeding of the Royal Society (A), 1929, **123**, pp 440-465.
27. ROSEN, A. and GRABER, A. Free wake model of hovering rotors having straight or curved blades, *J American Helicopter Soc*, 1988, **33**, (3), pp 11-19.
28. RAND, O. and ROSEN, A. Efficient method for calculating the axial velocities induced along rotating blades by trailing helical vortices, *AIAA J of Aircr*, June 1984, **21**, pp 433-435.
29. LEISHMAN, J.G. *Principles of Helicopter Aerodynamics*, Cambridge Aerospace Series, Cambridge University Press.
30. LARRABEE, E.E. Practical design of minimum induced loss propellers, 1979, SAE 790585, Business Aircraft Meeting and Exposition, 3-6 April, 1979, Century II, Wichita.
31. CRIGLER, L.J. Application of Theodorsen's theory to propeller design, 1948, NACA Report 924.
32. MCLEMORE, H.C. and CANNON, C.M. Aerodynamic investigation of a four-blade propeller operating through an angle-of-attack range from 0º to 180º, June 1954, NACA Technical Note No 3228.

https://doi.org/10.1017/S0001924000002669 Published online by Cambridge University Press